

# Constraining pion interactions at very high energies by cosmic ray data

Sergey Ostapchenko<sup>1,2</sup> and Marcus Bleicher<sup>1,3</sup>

<sup>1</sup>*Frankfurt Institute for Advanced Studies, 60438 Frankfurt am Main, Germany*

<sup>2</sup>*D.V. Skobeltsyn Institute of Nuclear Physics, Moscow State University, 119992 Moscow, Russia*

<sup>3</sup>*Institute for Theoretical Physics, Goethe-Universitat, 60438 Frankfurt am Main, Germany*

October 15, 2018

## Abstract

We demonstrate that a substantial part of the present uncertainties in model predictions for the average maximum depth of cosmic ray-induced extensive air showers is related to very high energy pion-air collisions. Our analysis shows that the position of the maximum of the muon production profile in air showers is strongly sensitive to the properties of such interactions. Therefore, the measurements of the maximal muon production depth by cosmic ray experiments provide a unique opportunity to constrain the treatment of pion-air interactions at very high energies and to reduce thereby model-related uncertainties for the shower maximum depth.

## 1 Introduction

Experimental studies of high energy cosmic rays (CRs) are traditionally performed using extensive air shower (EAS) techniques: the properties of the primary CR particles are reconstructed from measured characteristics of nuclear-electromagnetic cascades induced by their interactions in the atmosphere. This naturally implies the importance of detailed Monte Carlo simulations of the EAS development, particularly, of its backbone – the cascade of nuclear interactions of both, the primary particles and of the secondary hadrons produced. Thus, the very success of these experimental studies depends crucially on the accuracy of the modeling of hadron-air collisions at high energies. This is especially so for measurements of the

nuclear composition of ultra-high energy cosmic rays (UHECRs). The primary CR composition is the key observable for discriminating between different astrophysical models for the origin of the UHECRs and is of utmost importance for revealing the nature of UHECR sources (for recent reviews, see [1, 2]).

Typically, one chooses between two main experimental procedures [3, 4]. In the first case, one deals with the information obtained by scintillation detectors positioned at ground. The energy of the primary particle is reconstructed from the measured lateral density of charged particles (mostly, electrons and positrons) while the particle type is inferred from the relative fraction of muons, compared to all charged particles at ground. Alternatively, one may study the longitudinal EAS development by measuring fluorescence light produced by excited air molecules at different heights in the atmosphere. Here dedicated fluorescence telescopes are employed. In the latter case, the primary energy is related to the total amount of fluorescence light emitted. In turn, the particle type may be determined from the measured position of the shower maximum  $X_{\max}$  – the depth in the atmosphere (in  $\text{g}/\text{cm}^2$ ), where the number of ionizing particles reaches its maximal value.

Not surprisingly, the observables used to determine the primary particle type – the lateral muon density and the EAS maximum position  $X_{\max}$  – appear to be very sensitive to details of high energy hadronic interactions [5]. More precisely,  $X_{\max}$  depends strongly on the properties of the primary particle interaction with air nuclei: the inelastic cross section and the forward

spectra of secondary hadrons produced. In turn, the EAS muon content is formed in a multistep cascade process, driven mostly by interactions of secondary pions and, to a smaller extent, kaons with air. Here, we are going to demonstrate that present model predictions for the average shower maximum depth also depend noticeably on the model treatment of pion-air collisions. Moreover, due to a reduction of uncertainties related to the description of very high energy proton-proton and proton-nucleus interactions, caused by a more reliable model calibration with the data of the Large Hadron Collider (LHC), the treatment of pion-nucleus collisions becomes the dominant source of model uncertainty concerning  $X_{\max}$  predictions. We will demonstrate how this can be constrained by measurements of the maximal muon production depth in air showers.

## 2 Uncertainties of model predictions for $X_{\max}$

By far, the most suitable EAS parameter for studying primary CR composition is the shower maximum depth  $X_{\max}$ . Apart from the possibility to measure it reliably by modern air fluorescence detectors, the uncertainties of the respective model predictions have been greatly reduced with the start of LHC. Especially, the precise measurements of the total and elastic proton-proton cross sections by the TOTEM and ATLAS experiments [6, 7] provided strong constraints for the models. Another potential source of uncertainty for  $X_{\max}$  is related to its sensitivity to the rate of inelastic diffraction in proton-proton and proton-nucleus collisions. Diffraction largely dominates the shape of the very forward spectra for secondary particle production, which in turn makes a strong impact on the longitudinal EAS development. This has been investigated in Ref. [8] in the framework of the QGSJET-II-04 model [9], in view of recent studies of diffraction at LHC. The obtained characteristic uncertainty for  $X_{\max}$  amounted to 10 g/cm<sup>2</sup>, being thus comparable to the accuracy of the shower maximum measurements.

However, present differences between various calculations of  $X_{\max}$  are substantially larger, as illustrated in Fig. 1 (left) with the corresponding results of the QGSJET-II-04, EPOS-LHC [10],

and QGSJET [11, 12] models.<sup>1</sup> Particularly surprising is the difference between the QGSJET-II-04 and EPOS-LHC predictions as both models have been recently updated using LHC data. Thus, the question arises if the analysis of Ref. [8] was not general enough or the position of the shower maximum depends on some other characteristics of hadronic interactions, not well constrained by present LHC data.

To reveal the interaction features which are responsible for the above-discussed differences in  $X_{\max}$  predictions, we are going to employ a “cocktail” model approach: using QGSJET-II-04 to describe some selected interactions of hadrons in the atmospheric cascades or some particular features of the primary interaction, while treating the rest with one of the other two models.<sup>2</sup> As the first step, we apply QGSJET-II-04 to determine the position of the primary particle interaction in the atmosphere and to describe the production of secondary nucleons in this interaction; all other characteristics of the first proton-air collision and all the subsequent interactions of secondary hadrons in the cascade are treated using EPOS-LHC. This way we check the sensitivity of the calculated  $X_{\max}$  to the model differences concerning the proton-air cross section and the predicted nucleon spectra, which thus comprise the effects of the inelastic diffraction. The obtained  $X_{\max}$  shown by the blue dotted-dashed line in Fig. 1 (left) differs from the original EPOS-LHC results by not more than 5 g/cm<sup>2</sup>, which is well within the uncertainty range obtained in Ref. [8].

Next, we apply QGSJET-II-04 to describe all the characteristics of the primary interaction, while treating the rest of the hadron cascade using EPOS-LHC. The obtained  $X_{\max}$  shown by the blue dashed line in Fig. 1 (left) is shifted further towards the QGSJET-II-04 results by up to 5 g/cm<sup>2</sup>. This additional shift is explained by somewhat harder spectra of secondary mesons, most importantly, of secondary pions in EPOS-LHC, compared to QGSJET-II-04. Here we actually observe an important change in the

<sup>1</sup>Here and in the following the calculations of EAS development are performed using the CONEX code [13].

<sup>2</sup>We restrict our analysis to the case of proton-initiated air showers: For average characteristics of nucleus-induced EAS, the “superposition” model works quite well [11, 14, 15]. E.g., for the energy dependence of  $X_{\max}$  for iron- and proton-induced EAS, the relation  $X_{\max}^{\text{Fe}}(E_0) = X_{\max}^p(E_0/56)$  holds to a good accuracy.

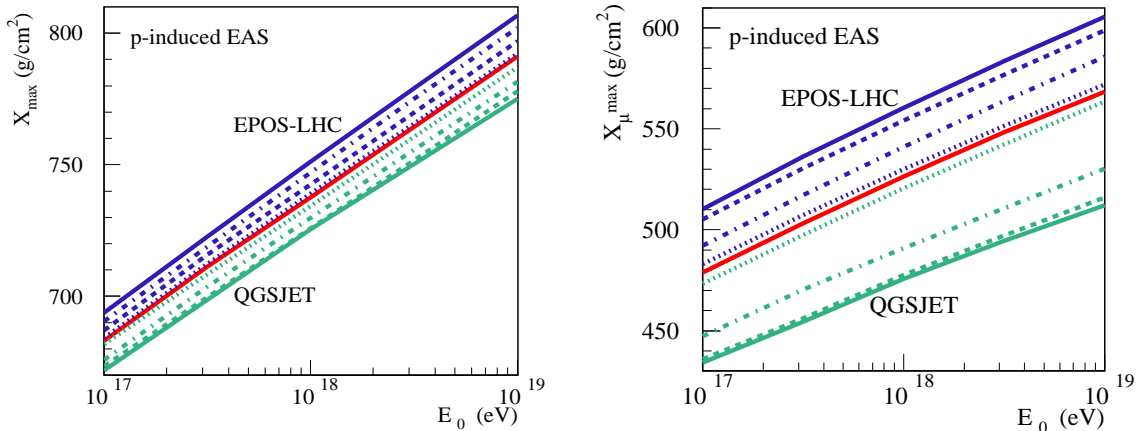


Figure 1: Primary energy dependence of  $X_{\max}$  (left) and of  $X_{\max}^{\mu}$  for  $E_{\mu} \geq 1$  GeV (right) for proton-initiated vertical EAS, calculated using the EPOS-LHC, QGSJET-II-04, and QGSJET models (respectively top blue, middle red, and bottom green solid lines), or applying mixed model descriptions, as explained in the text (dashed, dotted-dashed, and dotted lines).

physics of the hadronic cascade in the atmosphere. At lower energies, there is a very pronounced “leading nucleon” effect, i.e. most energetic secondary particles in proton-air collisions are typically protons or neutrons (produced either directly or via decays of hyperons and resonances). On the other hand, in the very high energy limit the energy loss of leading nucleons is noticeably higher and the most energetic secondary hadron may well be a pion or a kaon, which results in a stronger sensitivity of  $X_{\max}$  calculations to the corresponding production spectra. We also repeat the same calculation describing secondary hadron interactions in the cascade with QGSJET, the results being plotted by the green dashed line in Fig. 1 (left). In this case, the difference with the pure QGSJET-based calculation does not exceed 3 g/cm<sup>2</sup>, which is due to the fact that forward particle spectra in proton-air collisions are rather similar in QGSJET and QGSJET-II-04.

Thus, there remain large differences between the two dashed lines in Fig. 1 (left) and the results of QGSJET-II-04, which arise from the model treatments of pion- and kaon-air interactions. In the particular case of QGSJET, this amounts to 10 – 13 g/cm<sup>2</sup>, i.e. to  $\simeq 80\%$  of the difference between QGSJET and QGSJET-II-04, and is mainly related to the larger pion-air cross section and softer production spectra for secondary mesons, predicted by QGSJET. The larger cross section is responsible for  $\simeq 20\%$

of the difference, as is illustrated by the green dotted-dashed line in Fig. 1 (left), obtained by using QGSJET-II-04 both for the primary interaction and for the inelastic cross sections for all the secondary hadron-air collisions in the cascade. In turn, applying QGSJET-II-04 to describe also pion and kaon spectra in pion-air collisions produces an additional 35 – 50% effect, as shown by the green dotted line in Fig. 1 (left).

In case of EPOS-LHC, the remaining  $\simeq 35\%$  difference with the QGSJET-II-04 results is both due to a copious production of baryon-antibaryon pairs in pion- and kaon-air collisions and due to harder (anti-)baryon spectra in EPOS-LHC [16]. These features lead to a slower energy dissipation from the hadronic cascade, hence, to an elongation of the shower profile. Indeed, if we apply QGSJET-II-04 to describe both the primary interaction and the production of nucleons and antinucleons in all the secondary pion- and kaon-air collisions, while treating the rest with EPOS-LHC, the obtained  $X_{\max}$  shown by the blue dotted line in Fig. 1 (left) practically coincides with the QGSJET-II-04 results.

Let us now determine the energy range of pion- and kaon-air collisions which are most relevant for the above-discussed model dependence of  $X_{\max}$  calculations. To this end, we apply QGSJET-II-04 to treat all hadronic interactions in the cascade above some “transition” energy  $E_{\text{trans}}$ , while describing hadron-air collisions at  $E < E_{\text{trans}}$  using either EPOS-LHC or

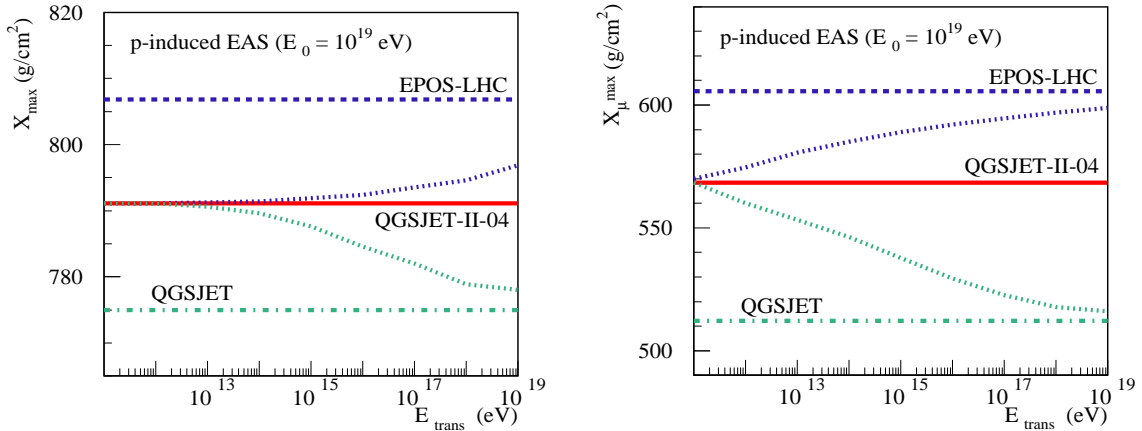


Figure 2:  $E_{\text{trans}}$ -dependence of  $X_{\text{max}}$  (left) and of  $X_{\text{max}}^{\mu}$  for  $E_{\mu} \geq 1$  GeV (right) for proton-initiated vertical EAS of energy  $10^{19}$  eV, calculated using QGSJET-II-04 for hadronic interactions at  $E > E_{\text{trans}}$  and applying EPOS-LHC or QGSJET at  $E < E_{\text{trans}}$  - respectively blue and green dotted lines. The predictions of the QGSJET-II-04, EPOS-LHC, and QGSJET models are shown by the red solid, blue dashed, and green dotted-dashed lines respectively.

QGSJET. The obtained dependence of the calculated  $X_{\text{max}}$  on  $E_{\text{trans}}$  for the two cases is shown in Fig. 2 (left) by respectively blue and green dotted lines for  $E_0 = 10^{19}$  eV. Not surprisingly, the model differences for the predicted  $X_{\text{max}}$  are due to very high energy pion- and kaon-air interactions, which is reflected in the strong  $E_{\text{trans}}$ -dependence in the corresponding energy range. Indeed, as the longitudinal charged particle profile in EAS is dominated by the contribution of electrons and positrons,  $X_{\text{max}}$  may be influenced by pion- and kaon-air interactions only in the beginning of the hadronic cascade, before most of the energy of the primary particle is channelled into secondary electromagnetic cascades.

### 3 Relation to maximal muon production depth

As demonstrated in Section 2, a large part of the model uncertainty for the predicted  $X_{\text{max}}$  is related to the treatment of pion-air collisions at very high energies. As no accelerator experiments with a very high energy pion beam are foreseen, this may constitute a serious obstacle for improving the accuracy of  $X_{\text{max}}$  calculations and thus may hamper further progress in experimental studies of UHECR composition.

However, the treatment of pion-nucleus interactions can be constrained indirectly by study-

ing other characteristics of very high energy EAS. Recently, the Pierre Auger experiment measured the maximal muon production depth in EAS,  $X_{\text{max}}^{\mu}$  - the depth in the atmosphere (in  $\text{g}/\text{cm}^2$ ), where the rate of muon production via decays of pions and kaons reaches its maximal value [17]. In particular, one observed a strong contradiction between the results of EAS simulations with EPOS-LHC and the experimental data: the measured  $X_{\text{max}}^{\mu}$  was substantially smaller than predicted by that model, even if the heaviest primary CRs were considered.

There are both similarities and differences concerning the relation of  $X_{\text{max}}$  and  $X_{\text{max}}^{\mu}$  to the properties of hadron-air collisions. Obviously, both characteristics are sensitive to the position  $X_0$  of the primary particle interaction in the atmosphere, which depends on the respective inelastic cross section: fluctuations of  $X_0$  shift the whole cascade upwards and downwards in the atmosphere and thus do so for  $X_{\text{max}}$  and  $X_{\text{max}}^{\mu}$  for a particular shower. However, in contrast to  $X_{\text{max}}$ ,  $X_{\text{max}}^{\mu}$  is much less sensitive to hadron production in the primary interaction. The EAS muon content rather depends on the multistep hadronic cascade in which the number of pions and kaons increases in an avalanche way until the probabilities for their decays become comparable to the ones for interactions. For charged pions, this happens when their energies approach the corresponding critical energy,

$E_{\text{crit}}^{\pi^\pm} \simeq 80$  GeV [18]. The maximum of the muon production profile is close to this turning point.

As a consequence,  $X_{\text{max}}^\mu$  is very sensitive to the forward spectral shape of secondary mesons in pion-air collisions: producing in each cascade step a meson of a slightly higher energy would mean that a larger number of cascade branchings is required for reaching the critical energy, with the result that the maximum of the muon production profile will be observed deeper in the atmosphere. A similar effect may be produced by a smaller pion-air cross section as this would increase the pion mean free pass and thereby elongate the muon production profile. However, there is another potential mechanism which may influence model predictions for  $X_{\text{max}}^\mu$ , namely, a copious production of baryon-antibaryon pairs in pion-air interactions. Indeed, (anti-)nucleons do not decay,<sup>3</sup> hence, they continue to interact even when their energies fall below 100 GeV, producing additional generations of secondary hadrons in the cascade. Muons emerging from decays of secondary pions and kaons created in interactions of such low energy (anti-)nucleons contribute to the elongation of the muon production profile and give rise to larger values of  $X_{\text{max}}^\mu$ . It is noteworthy that the respective effect is noticeable if (and only if) the yield of baryon-antibaryon pairs in pion-air collisions is comparable to the one of secondary pions.

For the calculated  $X_{\text{max}}^\mu$  (for muon energies  $E_\mu \geq 1$  GeV), we observe substantially stronger model dependence than for  $X_{\text{max}}$ , as demonstrated in Fig. 1 (right). To reveal the physics behind, we use the same “cocktail” model approach as in Section 2. First, we apply QGSJET-II-04 to describe all the characteristics of the primary interaction, while treating the rest of the hadron cascade using either EPOS-LHC or QGSJET, the results shown respectively by the blue and green dashed lines in Fig. 1 (right). As expected, the obtained  $X_{\text{max}}^\mu$  deviates only slightly from the original model calculations: the difference between the solid and dashed blue lines does not exceed 7 g/cm<sup>2</sup>, while being even smaller for QGSJET (solid and dashed green lines). Indeed, the bulk of the differences between the model predictions for  $X_{\text{max}}^\mu$  is due to secondary (mostly pion-air) interactions in the cascade. In case of QGSJET,

<sup>3</sup>Life time of relativistic neutrons exceeds by many orders of magnitude the time scale for EAS development.

this is mainly caused by somewhat larger inelastic pion- and kaon-air cross sections and softer meson spectra predicted by that model. The first effect is responsible for  $\simeq 25\%$  of the difference between QGSJET and QGSJET-II-04. This is illustrated by the green dotted-dashed line in Fig. 1 (right), which is obtained applying QGSJET-II-04 to describe both the primary interaction and the inelastic cross sections for all the secondary hadron-air collisions in the cascade, while treating hadron production in secondary hadron-air interactions with QGSJET. On the other hand, using QGSJET-II-04 results also for the pion and kaon spectra in pion-air collisions produces an additional  $\simeq 60\%$  effect which thus covers the most of the difference of the two models’ predictions for  $X_{\text{max}}^\mu$ , as shown by the green dotted line in Fig. 1 (right).

In turn, the largest part of the difference between EPOS-LHC and QGSJET-II-04 ( $\simeq 35 - 40\%$ ) is due to the copious production of baryon-antibaryon pairs in the former model. This is illustrated by the blue dotted-dashed line in Fig. 1 (right), which is obtained applying QGSJET-II-04 to describe both the primary interaction and the production of nucleons and antinucleons in all the secondary pion-air collisions, while treating the rest with EPOS-LHC. The remaining  $\simeq 30 - 35\%$  difference between the two models is due to harder spectra of secondary mesons in EPOS-LHC for pion- and kaon-air interactions. Indeed, using QGSJET-II-04 results both for the primary interaction and for hadron spectra in pion- and kaon-air collisions, we obtain the energy dependence of  $X_{\text{max}}^\mu$ , shown by the blue dotted line in Fig. 1 (right), which is very close to the pure QGSJET-II-04 calculation.

Finally, let us check the energy range of pion- and kaon-air collisions which impact  $X_{\text{max}}^\mu$ . As in Section 2, we apply QGSJET-II-04 to treat hadronic interactions at  $E > E_{\text{trans}}$ , while describing hadron-air collisions at  $E < E_{\text{trans}}$  using either EPOS-LHC or QGSJET. The obtained dependence of  $X_{\text{max}}^\mu$  on  $E_{\text{trans}}$  for the two cases is shown in Fig. 2 (right) by respectively blue and green dotted lines for  $E_0 = 10^{19}$  eV. Similarly to the  $X_{\text{max}}$  case, the range of relevant pion- and kaon-air collisions extends to very high energies, as reflected by the observed  $E_{\text{trans}}$ -dependence of the calculated  $X_{\text{max}}^\mu$ . On the other hand, this energy range is significantly broader than in the case of  $X_{\text{max}}$  because all the stages of the

hadronic cascade development, down to the pion critical energy, contribute here.

## 4 Conclusions

We have demonstrated that a substantial part of present uncertainties concerning model predictions for the average EAS maximum depth is related to the modeling of very high energy pion-air collisions. We traced down the sources of these uncertainties to differences in model predictions concerning the inelastic cross sections and production spectra of mesons and (anti-)nucleons in pion-nucleus interactions. On the other hand, our analysis revealed an even stronger sensitivity of the calculated maximal muon production depth in air showers to these interaction characteristics. Thus, measurements of  $X_{\max}^{\mu}$  by CR experiments have a good potential to constrain the treatment of pion-air interactions in the very high energy range and to reduce thereby model-related uncertainties for  $X_{\max}$ . In particular, the results of the Pierre Auger experiment disfavor a copious production of baryon-antibaryon pairs, predicted by the EPOS-LHC model, and reduce thereby the range of model uncertainties for  $X_{\max}$ .

In conclusion,  $X_{\max}^{\mu}$  measurements by CR experiments provide an important complement to LHC studies for constraining the models of high energy hadronic interactions. Further experimental progress in both directions, along with improvements in the interaction modeling, will contribute to the resolution of the UHECR composition puzzle.

## Acknowledgments

The authors acknowledge useful discussions with T. Pierog. This work was supported in part by Deutsche Forschungsgemeinschaft (project OS 481/1-1) and the State of Hesse via the LOEWE-Center HIC for FAIR.

## References

- [1] K. Kotera and A. V. Olinto, *Ann. Rev. Astron. Astrophys.* **49**, 119 (2011).
- [2] P. Blasi, *Comptes Rendus Physique* **15**, 329 (2014).
- [3] M. Nagano and A. A. Watson, *Rev. Mod. Phys.* **72**, 689 (2000).
- [4] K.-H. Kampert and M. Unger, *Astropart. Phys.* **35**, 660 (2012).
- [5] R. Ulrich, R. Engel, and M. Unger, *Phys. Rev. D* **83**, 054026 (2011).
- [6] G. Antchev *et al.* (TOTEM Collaboration), *Europhys. Lett.* **101**, 21002 (2013); **101**, 21003 (2013); **101**, 21004 (2013); *Phys. Rev. Lett.* **111**, 012001 (2013).
- [7] G. Aad *et al.* (ATLAS Collaboration), *Nucl. Phys.* **B889**, 486 (2014).
- [8] S. Ostapchenko, *Phys. Rev. D* **89**, 074009 (2014).
- [9] S. Ostapchenko, *Phys. Rev. D* **83**, 014018 (2011); *EPJ Web Conf.* **52**, 02001 (2013).
- [10] T. Pierog, Iu. Karpenko, J. M. Katzy, E. Yatsenko, and K. Werner, *Phys. Rev. C* **92**, 034906 (2015).
- [11] N. N. Kalmykov and S. S. Ostapchenko, *Phys. Atom. Nucl.* **56**, 346 (1993).
- [12] N. N. Kalmykov, S. S. Ostapchenko, and A. I. Pavlov, *Nucl. Phys. Proc. Suppl.* **52B**, 17 (1997).
- [13] T. Bergmann, R. Engel, D. Heck, N. N. Kalmykov, S. Ostapchenko, T. Pierog, T. Thouw, and K. Werner, *Astropart. Phys.* **26**, 420 (2007).
- [14] N. N. Kalmykov and S. S. Ostapchenko, *Sov. J. Nucl. Phys.* **50**, 315 (1989).
- [15] J. Engel, T. K. Gaisser, P. Lipari, and T. Stanev, *Phys. Rev. D* **46**, 5013 (1992).
- [16] T. Pierog and K. Werner, *Phys. Rev. Lett.* **101**, 171101 (2008).
- [17] A. Aab *et al.* (Pierre Auger Collaboration), *Phys. Rev. D* **90**, 012012 (2014); *ibid.*, **90**, 039904 (2014); *ibid.*, **92**, 019903 (2015).
- [18] T. K. Gaisser, *Cosmic Rays and Particle Physics* (Cambridge University Press, Cambridge, England 1990).